The study of volumetric wearing of PCBN/W-Re composite tool during Friction Stir Processing of pipeline steels (X70) plates

Rafael A. R. Giorjão[1,2], *Julian A. Avila D.[3], Julian David Escobar Atehortua[2], Victor Ferrinho Pereira[1], Ricardo Reppold Marinho[5], Marcelo Torres Piza Paes[5], Eduardo B. Da Fonseca[1,4], Alex M. S. Costa[6], *Maysa Terada[7]

1. Brazilian Nanotechnology National Laboratory (CNPEM), Rua Giuseppe Máximo Scolfaro, 10.000 Polo II de Alta Tecnologia de Campinas, CEP 13083-970 Campinas, SP, Brazil.
2. Welding Engineering Department, The Ohio State University, Columbus, OH, USA
3. São Paulo State University (UNESP), Campus of São João da Boa Vista, Av. Profª Isette Corrêa Fontão, 505, Jardim das Flores, 13876-750 - São João da Boa Vista, SP, Brazil
4. School of Mechanical Engineering, University of Campinas (UNICAMP), Rua Mendeleyev 200, Campinas, SP, 13083860, Brazil
5. PETROBRAS, CENPES, Av. Horácio Macedo 950, Rio de Janeiro, RJ 21941-915, Brazil
6. National Institute of Technology - INT, Rio de Janeiro, RJ, 20081-312, Brazil
7. SENAI Innovation Institute for advanced manufacturing and microfabrication. Rua Bento Branco de Andrade Filho,379. 04757-000, São Paulo, SP, Brazil

***Corresponding author**: Dr. Julián Ávila, julian.avila@unesp.br; Dr. Maysa Terada, maysa.terada@sp.senai.br

Short title: Volumetric and wear of PCBN tool during FSP of an HSLA steel.

ABSTRACT

Friction stir welding is a solid-state joining/processing technique that offers high strength and productivity, resulting in a microstructure similar to hot working cycles. However, high melting temperature metals such as steels cause excessive wear over welding tools, representing a significant economic issue. Most studies conducted in steels have used polycrystalline cubic boron nitride (PCBN) and W-Re composite tools, which offer a combination of high strength and hardness at high temperatures, along with high-temperature stability. However, even those tools are susceptible to tool wear. In the present study, experimental data was collected during friction stir processing of X70 grade pipeline steel plates, using W-Re and PCBN composite tools under well-controlled conditions. Profilometry and optical microscopy were used to quantify the volume loss at the welding tool due to the number of plunges and the welded distance. Torque and transverse force at the welding tool and the welded bead width were measured and related to the wear process. Tool contamination in boron-nitrogen particles and dissolved tungsten was identified at the stir and hard zones, more substantial at the latter.
Keywords: friction stir processing; pipeline steel, PCBN, wear, volume track

1. 1. Introduction

Friction stir welding (FSW) has found applications in various industries, including aerospace, automotive, and naval [1]. For the pipeline industry, FSW is highly energy efficient compared to conventional fusion welding processes, such as arc and laser beam welding, with a reduction in energy usage of 60 to 80% [2]. The traditional FSW tool consists of a shoulder and a pin; the shoulder predominantly generates frictional heat and prevents the expulsion of material from the weld zone. The tool's role is to provide sufficient plastic deformation to cause bonding across any pre-existing interfaces while stirring the material. Additionally, tool geometry must often facilitate a stable force or torque control scheme and be compatible with a range of plunge depths [1].

A proper selection of FSW tool material and design plays a crucial role in achieving suitable microstructures and mechanical properties in the welded joints. High melting point materials require tools made of cemented carbides, mainly WC-Co [3,4], Polycrystalline Cubic Boron Nitride (PCBN) [5–7], or refractory metal alloys based on W [8]. Carbides are commonly used as machining tools as they provide high wear resistance and good fracture toughness for FSW pin/shoulder at room temperature [9]. PCBN, developed initially for turning and machining tool steels, cast irons, and superalloys, is currently a well-accepted FSW tool due to its strength, hardness, and

high-temperature stability [1]. The FSW tool is supposed to be non-consumable; yet, they suffer wear and dimensional changes over several welding passes [10–12], increasing the probability of defect formation and possibly impairing the joint quality.

Additionally, particles of the tool can be incorporated in the stir zone, as observed by several authors [5,13–16]. In some applications, this may be acceptable. In other cases, the embedded tool particles present a significant detrimental effect on the joint properties.

The wear mechanism depends on the interaction between the workpiece and the tool, the tool geometry, and the welding parameters. The wear rate of PCBN tools is mainly caused by adhesive wear, also known as scoring, galling, or seizing, at low tool rotation, or abrasive wear at high tool rotation [17]. Park et al. [5] suggested the presence of Cr-rich borides in the stir zone at the advancing side (SZ-AS) in austenitic stainless steels were associated with PCBN tool wear. As the Cr-rich borides consume the Cr, a Cr-depleted zone appears at the vicinities and can trigger the sigma phase. Hanke et al. [13] showed that material flows at high temperatures under high rotational speed caused severe tool wear. Barnes et al. [11] found that after a welded length of 5 m, all the features on a 6-mm PCBN pin and shoulder were completely worn. Almoussawi *et al.* [16] studied the tool wear of PCBN tools on DH36 and EH46 steels. They reported a relationship between wear and higher spindle speeds due to the W-Re binder softening and higher BN particle presence. Also, wear was exacerbated close to the shoulder and tip of the tools.

The tool wear also represents an impact on the cost of the weld [18]. Cost-effective and long-life tools are available for the FSW of aluminum but not for the commercial application of FSW to high strength materials. PCBN, for example, is expensive due to the high temperatures and pressures required in its manufacture [18]. Understanding the tool life behavior during welding of harder alloys is a critical step for future large-scale applications.

The present paper investigates the PCBN-W-Re composite tool wear during friction stir processing of API-5L-X70 grade pipeline steel plates. The volume loss at the tool, the welding torque, transverse force during welding, and the corresponding welded bead width were studied as a function of the number of plunges and total welded length. Additionally, tool contamination at the stir and hard zones was characterized by SEM and EDS.

2. Experimental Procedure

The wear process of a PCBN-W-Re (70%-vol. PCBN/ 30%-W-Re) tool, associated with steel friction stir processing, was studied under well-controlled

conditions. Four identical tools, namely A, B, C, and D, were used. The tool probe's geometry details (the most critical part of the present study) are presented in Figure 1. The probe is composed of a shoulder and a 9.5-mm step-spiral conical shape pin. Additional information about the tool geometry can be found in [19].

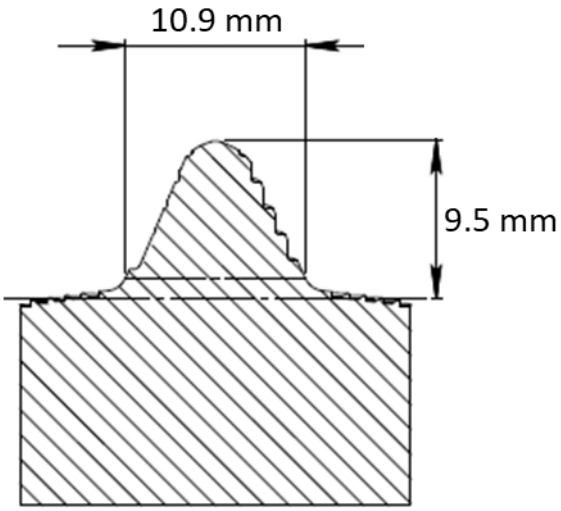

Figure 1: Cross-section of PCBN-W-Re tool's probe geometry

Consecutive 100-mm processing weld beads were performed along with several 17-mm thick API-5L-X70 grade pipeline steel plates. A total of three evenly distributed weld beads were performed per plate, with no bead overlap, and both sides of the plates were used. During welding, a longitudinal speed of 100 mm.min-1, a rotation speed of 300 RPM and an axial force of 32 kN were used. These parameters successfully provided a good superficial aspect without internal defects [20]. The welding parameters were kept constant along with the experiments. The steel chemical composition is shown in Table 1.

Table 1: Chemical composition of an API-5L-X70 grade pipeline steel in wt.%. * indicates ppm.

C	Si	Mn	Nb	Ni	Mo	P	N*	B*	S*	Ti	V	Fe
0.083	0.16	1.65	0.045	0.23	0.003	0.012	<5	<5	60	0.012	0.049	Bal.

An S-Neox non-contact 3D Surface Profiler was used to capture the probe profile, producing a 3D model using a focal variation technique. Focus-Variation integrates the small depth of an optical system's field along the scanning direction to create a well-focused image. The dimensional changes of the tools were measured after three consecutive weld beads, i.e., every 300 mm weld length, until the tool's catastrophic

failure. Figure 2 shows the welding tool schematics before being subjected to wear. The evaluated region is the PCBN-W-Re probe, which is in direct contact with the workpiece. The selected volume evaluated is shown in Figure 2, which consists of a 22 mm radius centered in the pin. Attention was taken to keep the tool surface clean during measurements, using acetone after each welding pass.

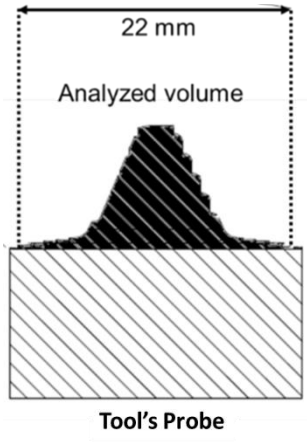

Figure 2: Tool's probe and respective evaluated region.

Cross-sections from the welded plates were prepared by standard metallographic procedures, including mechanical grinding and polishing up to 1 µm diamond suspension for SEM, OM, and EDS. The electron microscopy work was conducted with the SEM/EBSD FEI ® Quanta 650FEG available at LNNano, Campinas.

A SpectroMaxx arc spark optical emission spectrometer was used to measure the chemical composition of the base metal (BM), stir zone (SZ), and hard zone (HZ). The HZ is typically localized at the advancing side [7,20] or close to the joint's centerline; its formation has been related to high cooling rates [6] [19]. In a similar API 5L steel, hardness values of 272 Vickers were reported at the HZ [20]. At the same joint, the rest of the stir zone presented 234 Vickers and BM 231 Vickers. Additionally, a site-specific compositional analysis was conducted on the degree of tool contamination at the SZ and HZ. Figure 3 schematizes the tilt cuts specially made to increase the area of study of the hard zone. A total of 30 localized spark optical emission measurements, with a 3 mm diameter, were conducted in each region. Rhenium content could not be accurately determined due to the detection limit constraints of the equipment used in this work.

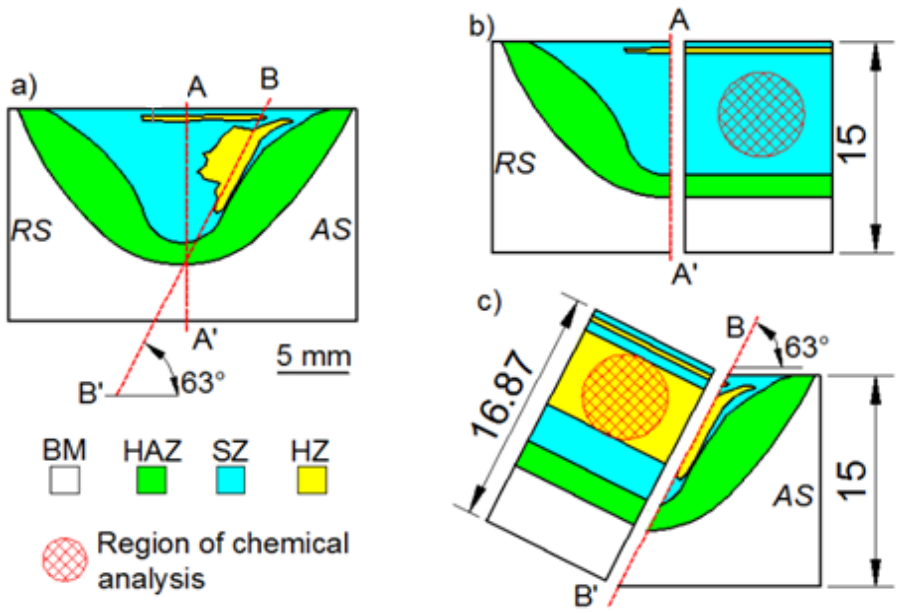

Figure 3. Cross-section of the welded joint showing: a) the sectioning of the regions of interest for chemical analysis, b) stir zone and cut A-A', and c) hard, zone and cut B-B'.

3. Results

3.1 Volumetric wear analysis

Figure 4 shows the model generated for the tool's probe (Tool A) in the as-received condition (Figure 4-a) and after 62 plunges (Figure 4-b). The 3D model provided by the surface profiler shows the wear in the threads and shoulder regions. The volume in mm^3 as a function of the plunging number and total welded distance is shown in Figure 5 for all four studied tools. The measurement deviation was ±1 mm^3.

The welding probes' wear rate was determined in this work as the volume loss curve slope. Tools A and B exhibited a similar wear rate of 0.017 $mm^3.mm^{-1}$. However, tool A produced 65 plunges and a 6400 mm length weld, the highest length between all tools. Tool B made 45 plunges and a 4500 mm length weld. Tool D presented the highest wear rate of 0.035 $mm^3.mm^{-1}$, performing 45 plunges and a 4300 mm in total weld length, the lowest performance of the four tools. Since all experimental conditions were kept constant, these results indicate the scattering of the probe wear performance associated with the processing of an API-5L-X70 grade pipeline steel.

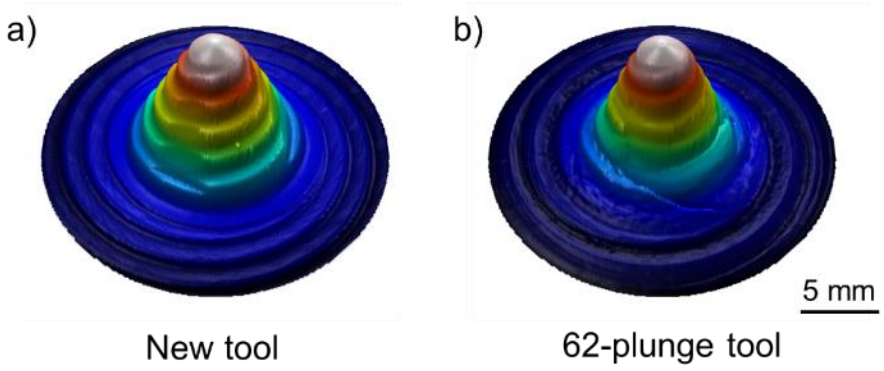

Figure 4: 3D model generated for the welding probes: a) as-received; b) after 62 plunges. The color pattern indicates the height difference using the shoulder as a reference (Dark blue).

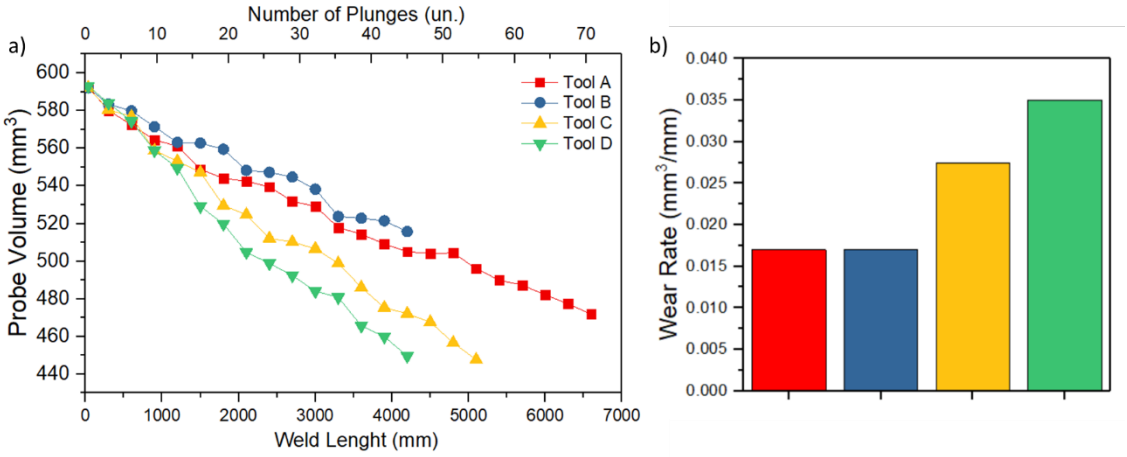

Figure 5: a) Probe volume (mm^3) as a function of the welded length and number of plunges performed, b) calculated tool's probe wear rate based on results shown in a).

3.2 Isometric view wear evaluation

Isometric views of the tool's probes were obtained, showing both pin and shoulder surfaces along with the wearing tests. Figure 6-a shows macrographs of the as-received condition. After 5, 10, 20, 40, and 60 plunges, the surface characterization is shown in Figure 6-b, c, d, e, and f, respectively. It is observed gradual wear localized at the threads along with the tool pin and shoulder. The probe's lines lose their original features in less than 20 plunges, promoting their smoothing profile. The region between the shoulder and the pin was the most affected. This behavior is related to the higher welding temperatures in this area, which promote the adhesive wear phenomena in the tool [21,22].

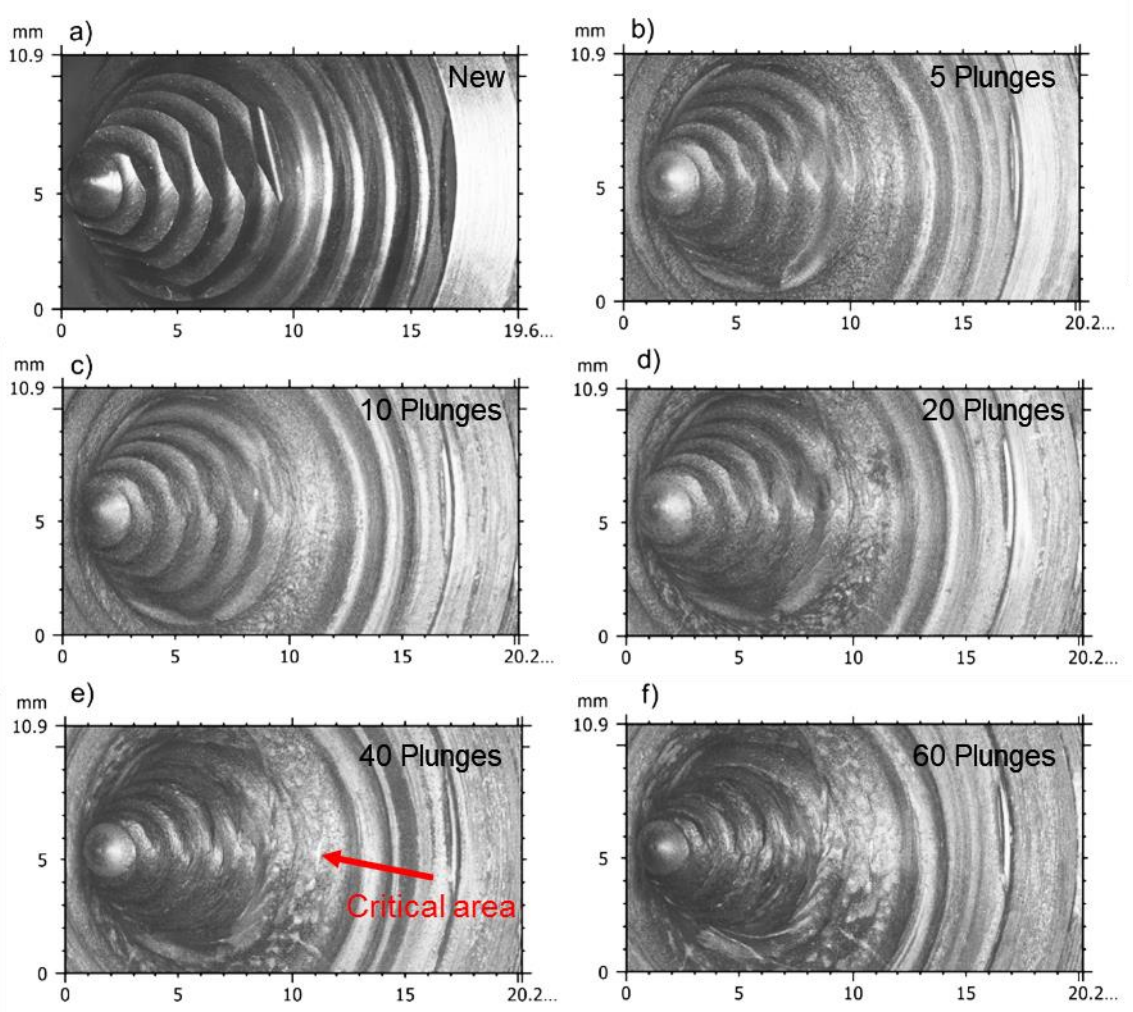

Figure 6: Isometric view of the tool's probe surface for the conditions: a) as-received, b) 5 plunges, c) 10 plunges, d) 20 plunges, e) 40 plunges, and f) 60 plunges. The red arrow indicates a region of critical wear concentration.

3.3 Side-view profile comparison

A detailed evolution of the tool wear performed by side-view profile analyses is shown in Figure 7. The wear process affected the pin shape preferentially in the diametral direction but did not affect its length. This phenomenon is explained by the pin's tip's relative velocity, which is close to zero, promoting less localized friction and wear. The diametral outermost regions of the pin and shoulder, where the highest relative velocities are present, suffered the most severe wear. This behavior was similar for the four studied tools.

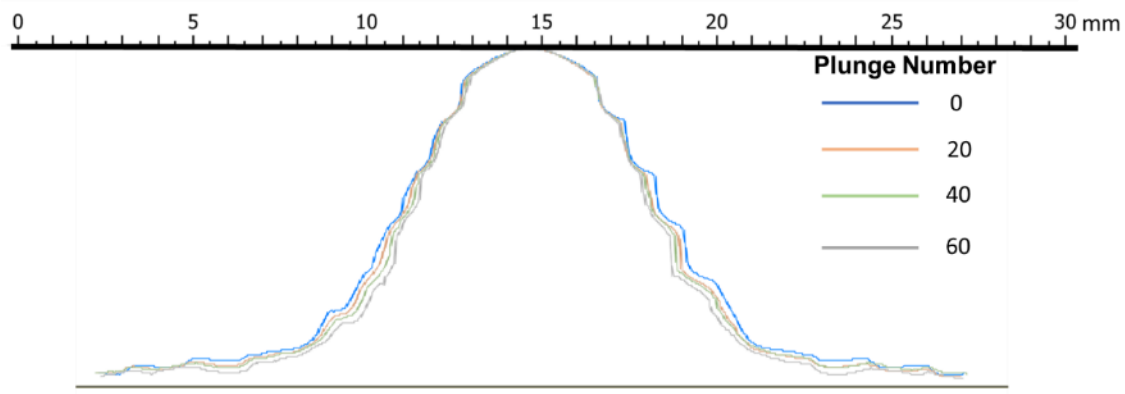

Figure 7: Tool A probe profiles for no wear condition, after 20 plunges, after 40 plunges, and after 60 plunges.

3.4 Torque and Forces

According to its wear state, the reaction forces were evaluated to understand the mechanical resistance between tool and workpiece. Axial and vertical forces, torque, and power can change depending on the welding input parameters, tool geometry, and material. Forces and torque in FSW can be considered as online indicators of weld quality [23]. Figure 8 shows the longitudinal forces relative to the welding direction and torque relative to the rotational speed. Results are presented for tool A in various stages of the wear process, i.e., the number of plunges. For comparison proposes, only the data related to the steady-state stage of the welding process was evaluated.

After reaching its steady-state condition, force and torque data showed less instability for the separate probe's wear conditions. It is noticed that the transversal force in the as-received tool is lower than for a worn condition. This behavior is related to the higher temperatures provided by the additional plastic deformation caused by threads. Threads provide additional material flow in the stir zone, causing an increment in materials temperature. A similar observation was made by Giorjao et al. [24], analyzing the tool geometry effect of friction stir welding in AZ31 Magnesium alloys using computational solid mechanics. In the study, a threaded pin, using the same parameter, promoted higher temperatures into the weld bead. As also pointed out by Hasan et al. [25] in a numerical study, strain rate and velocity distribution indicate a low, stirring action for worn tools, particularly near the weld root, potentially leading to defective weld joints. This low stirring contributes to a lower temperature underneath the worn tool [26]. The higher the process temperature, the less resistance to deformation the processed material demonstrates, and lower forces/torque are experienced, as seen in Figure 8-a and Figure 8-b. An increase in longitudinal forces may result in tool breakage due to excessive stress over time.

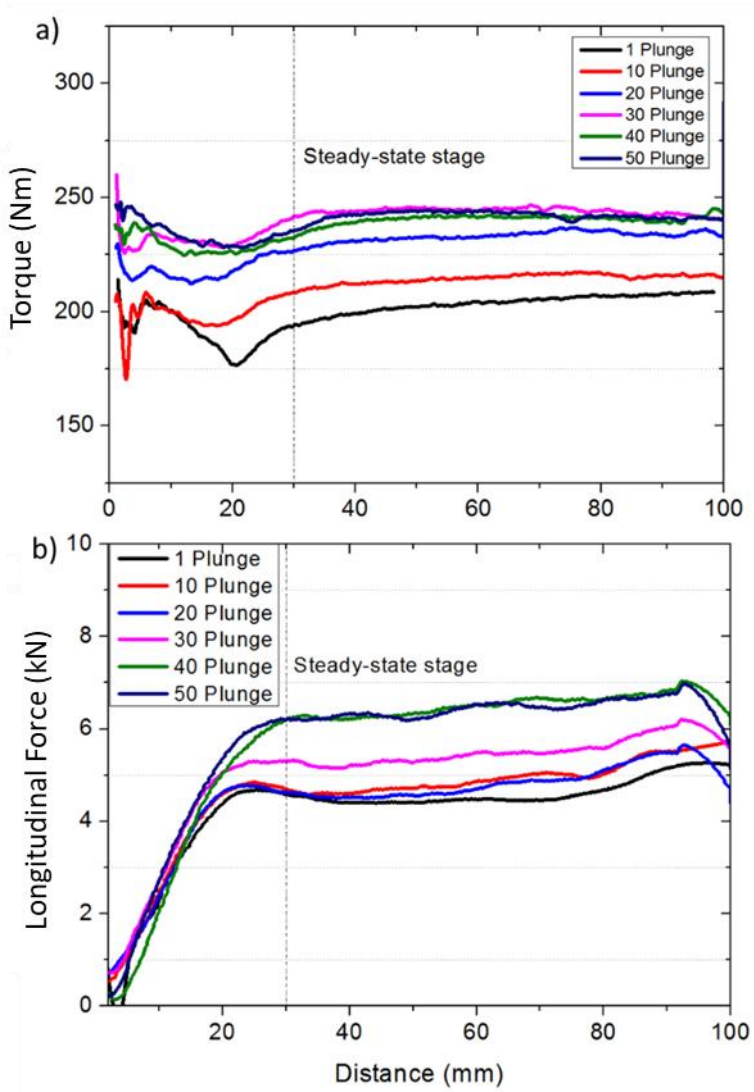

Figure 8: Tool response comparison in different worn conditions: a) Tool torque and b) longitudinal forces during friction stir welding

3.5 Weld Bead Width

Tool's capability to produce joints without defects was also evaluated. Superficial features of the weld bead were analyzed in distinct stages of tool life. Figure 9 shows the surface of the welds produced by a new tool and after 62 plunges. In all joints, a good surface appearance with some burr generation is noticed. However, it is possible to observe a slight decrease in the weld bead's width, which, as previously observed, is due to the reduction of the probe's profile. The width was measured and plotted in Figure 9-e, and the measured weld bead width decrease by 11.5%.

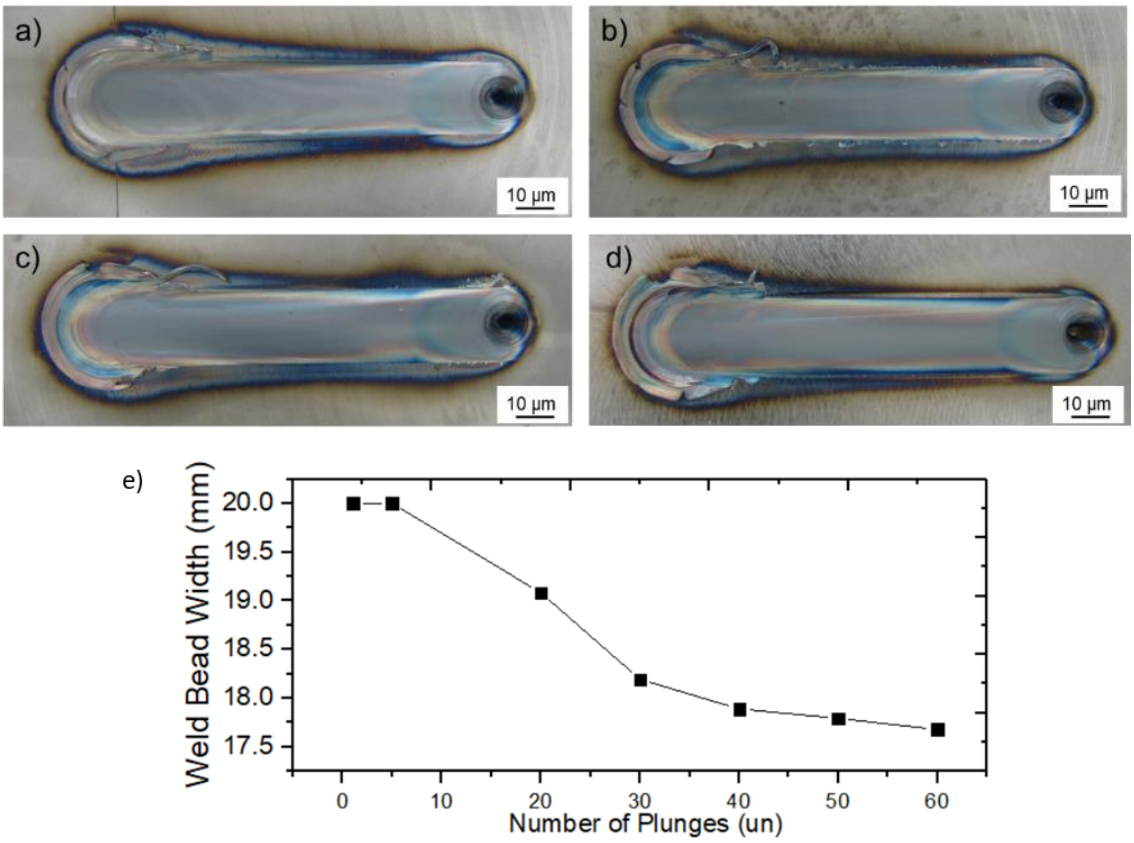

Figure 9: Weld bead superficial view for a new tool a), 20-plunge tool b), 40-plunge tool c), and 60-plunge tool d). e) Weld bead width in plunges performed

The macro-etched cross-section of the friction stir processed steel, obtained by a worn welding tool after 60 plunges, is shown in Figure 10-a. No defects, such as wormholes or voids, were found. The red circle in Figure 10-a indicates the region typically reported as the HZ [6,7,20]. Higher magnification of that region in Figure 9-b shows tool fragments concentrated along the macro-etched cross-section's dark-colored strips. EDS analysis indicated high boron and nitrogen contents at these particles, thus corresponding to a tool fragment deposited due to the wear process. Similar results were found by Park et al. [5], who identified boron and nitrogen in the SZ, resulting in the formation of Cr-rich borides in FSW of stainless steel using a PCBN-W-Re composite tool.

The high concentration of BN particles at the advancing side portion was detected and may be related to temperatures and materials flow due to the process itself. Several studies [19,27–29] show that the materials tend to move from the retreating side to the FSW's advancing side. Higher plastic deformation occurs at the AS, where the tool rotation and material flow directions are opposite [30]. Consequently, the preferential wear (presented in Figure 6), corresponding to the tool's upper portion (shoulder), geometrically coincided with the hard zone in the macro-etched cross-section.

The EDS analysis did not detect tungsten and Rhenium's presence, most likely due to the relatively small incorporation (below 1 wt.%) of these two into the steel workpiece.

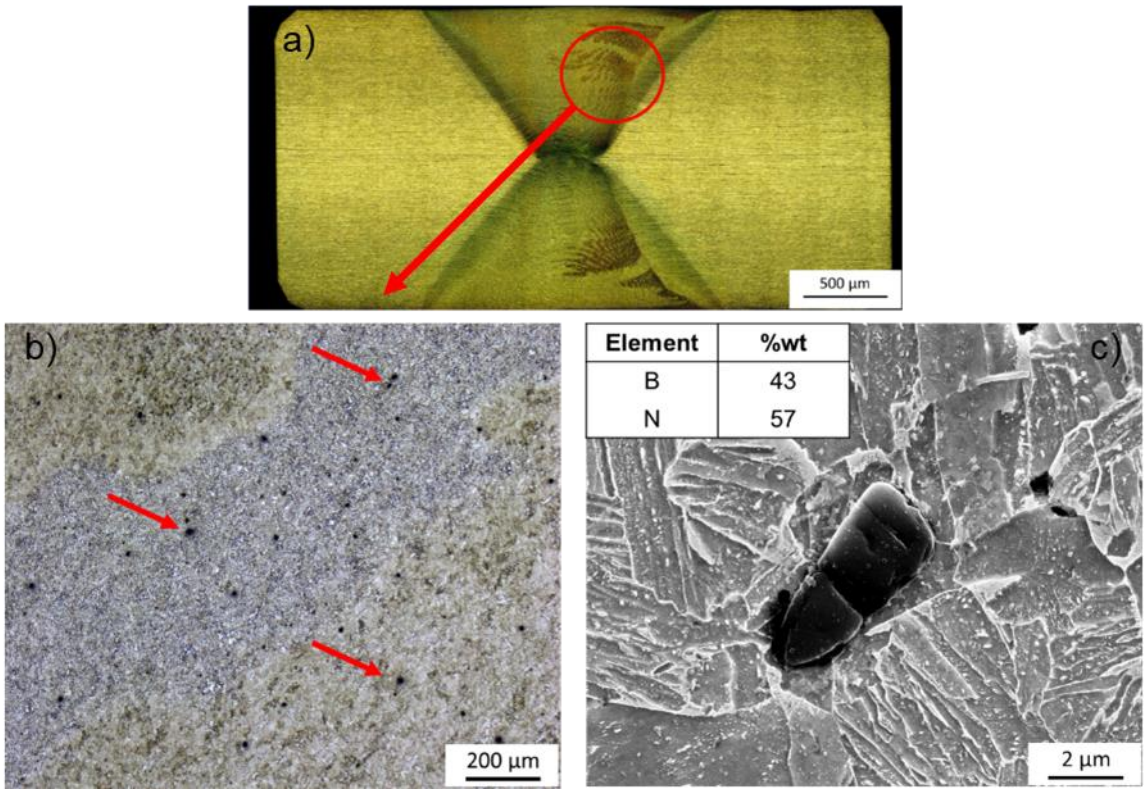

Figure 10. a) macro-etch of a cross-section of API X-70 grade pipeline steel produced with a welding tool after 60 plunges; b) Concentrated particles found at the advancing side portion of the stir zone, coinciding with the hard zone; c) Morphology and composition of a tool fragment inserted due to welding tool wear. The red circle indicates the hard zone; the red arrows indicate contamination particles

An additional test was performed to evaluate the probe's contamination on the steel. The chemical composition on the weld bead was measured by optical emission spectroscopy using tilted cuts (Figure 3) to maximize this microstructural region's area. Figure 11 shows the chemical analysis results for the BM, SZ, and HZ. The first two presented higher W, B, and N contents compared to the base metal. In this case, Re could not be accurately measured. The presence of W, B, and N was confirmed, especially in the HZ. These three elements can be directly related to contamination since the base metal's nominal composition does not contain alloying or micro-alloying additions of any of the welding tool elements.

It is not completely clear whether all W is found in a solid solution. According to Hanke et al. [13], who also found BN particles in friction stir welded Ni-alloys, diffusion occurs between BN and the adhering, hot plate material, thereby dissolving parts of the

BN crystals in the matrix. Furthermore, BN grain pull-outs representing a mechanical type of wear. Additionally, it is widely known that W, and especially B, have substantial effects on the hardenability of steels [31,32]. The addition of only 20 to 30 ppm of B can increase the hardenability factor 3 times in low carbon steels [32]. To determine the elemental distribution and carbide formation, further atom probe tomography and transmission electron microscopy analysis need to be performed.

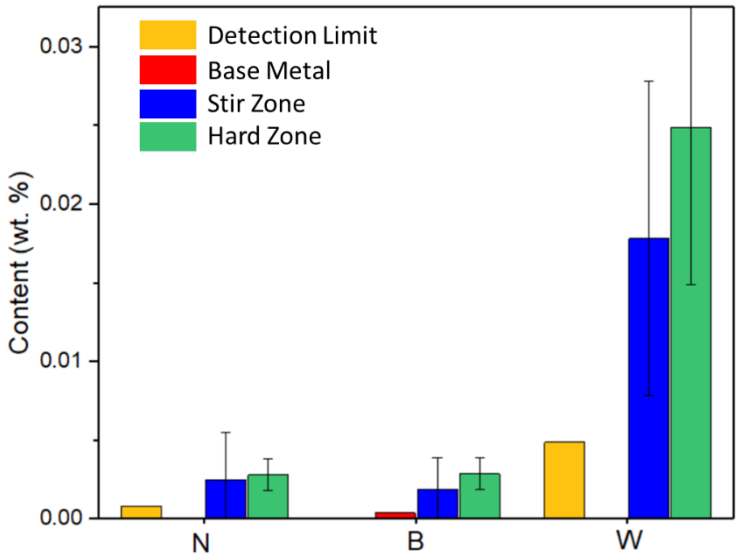

Figure 11. Chemical composition measured by optical emission spectroscopy at the base metal, stir zone, and hard zone after friction stir processing. The spectrometer detection limit is plotted for reference.

4 CONCLUSION

From this work, considerations were made regarding the tool wear behavior, its influence in weld bead condition, and tool response through its lifetime:

- Tools presented differences in wear rate behavior and total plunges before their breaking was noticed. The wear followed a constant rate, with no critical stages.
- The probe loses its original features along its lifetime, promoting the smoothing of the tool surface and tool tuning. The tuning phenomena cause less heat input and an increase in material resistance for the tool movement.
- As the tool loses its features, higher material resistance to deformation was observed. Worn tools generated less energy by friction and deformation, decreasing the temperature for the same parameters condition. The lower process temperature led to higher forces and torque experienced by the tool.

- Even worn tools provided a good surface appearance with a small burr generation. However, a slight decrease in the weld bead's width was noted due to the tool's reducing section promoted by its wear.
- SEM and energy dispersive X-ray spectroscopy analysis revealed boron-nitrogen particles on the weld bead's advancing side, which suggests being tool fragments. The founding may be related to the severe condition found in this region, which experiences higher temperatures than that on the retreating side. The EDS analysis did not detect w and Re.
- Although, the chemical analysis results for the base material (BM), stir zone (SZ), and hard zone (HZ). The SZ and HZ presented higher W, B, and N levels than the base metal nominal composition. The results suggest that W and Re may have diffused in solid solution along with the matrix, while the B and N are presented as fragments along the weld joint, especially in HZ.

ACKNOWLEDGEMENTS

The authors acknowledge Petrobras for financial support and Usiminas for the API-X70 plates donation. The authors would like to thank the Brazilian Nanotechnology National Laboratory (LNNano) for technical support during electron microscopy work.

Declarations:

- **Ethical Approval**

This research did not involve Human Participants or Animals; thus, an ethical approval is not necessary.

- **Consent to Participate:**

This research did not involve Human Participants; thus, a consent of participation is not necessary.

- **Consent to Publish:**

This research did not involve Human Participants; thus, a Consent to Publish is not necessary.

- **Authors Contributions:**
  - Rafael A. R. Giorjão: Investigation; Data curation; Formal analysis; Writing – original draft
  - Julian A. Avila D: Investigation; Writing - review & editing.
  - Julian David Escobar Atehortua: Investigation; Writing - review & editing.
  - Victor Ferrinho Pereira: Investigation.
  - Ricardo Reppold Marinho: Investigation.
  - Marcelo Torres Piza Paes: Investigation.
  - Eduardo B. da Fonseca: Investigation; Writing - review & editing.
  - Alex M. S. Costa: Investigation
  - Maysa Terada: Conceptualization; Supervision; Data curation; Formal analysis; Project administration; Writing

- **Funding:**
  The authors acknowledge Petrobras for financial support and Usiminas for the API-X70 plates donation.

- **Competing Interests:**
  The authors reported no potential conflict of interest.

- **Availability of data and materials:**
  The data that support the findings of this study are available from the corresponding author, [JA. Avila and M. Terada], upon reasonable request.

- **Disclosure statement:**
  No potential conflict of interest was reported by the authors.

REFERENCES

[1] R.S. Mishra, Z.Y. Ma, Friction stir welding and processing, Mater. Sci. Eng. R Reports. 50 (2005) 1–78. https://doi.org/10.1016/j.mser.2005.07.001.

[2] B.Y.J. Defalco, R. Steel, Friction stir process now welds steel pipe, Weld. J. (2009) 44–48.

[3] K.H. Song, K. Nakata, Mechanical Properties of Friction-Stir-Welded Inconel 625 Alloy, Mater. Trans. 50 (2009) 2498–2501. https://doi.org/10.2320/matertrans.M2009200.

[4] J. Wang, J. Su, R.S. Mishra, R. Xu, J.A. Baumann, Tool wear mechanisms in friction stir welding of Ti–6Al–4V alloy, Wear. 321 (2014) 25–32. https://doi.org/10.1016/j.wear.2014.09.010.

[5] S.H.C. Park, Y.S. Sato, H. Kokawa, Boride Formation Induced by pcBN Tool Wear in Friction-Stir-Welded Stainless Steels, Metall. Mater. Trans. A. 40 (2009). https://doi.org/10.1007/s11661-008-9709-9.

[6] T.W. Nelson, S.A. Rose, Controlling hard zone formation in friction stir processed HSLA steel, J. Mater. Process. Technol. 231 (2016) 66–74. https://doi.org/10.1016/j.jmatprotec.2015.12.013.

[7] T.F.A. Santos, T.F.C. Hermenegildo, C.R.M. Afonso, R.R. Marinho, M.T.P. Paes, A.J. Ramirez, Fracture toughness of ISO 3183 X80M (API 5L X80) steel friction stir welds, Eng. Fract. Mech. 77 (2010) 2937–2945. https://doi.org/10.1016/j.engfracmech.2010.07.022.

[8] B. THOMPSON, S.S. BABU, Tool Degradation Characterization in the Friction Stir Welding of Hard Metals, 89 (2010).

[9] Y.N. Zhang, X. Cao, S. Larose, P. Wanjara, Review of tools for friction stir welding and processing, Can. Metall. Q. 51 (2012) 250–261. https://doi.org/10.1179/1879139512Y.0000000015.

[10] H.J. Liu, J.C. Feng, H. Fujii, K. Nogi, Wear characteristics of a WC–Co tool in friction stir welding of AC4A+30vol%SiCp composite, Int. J. Mach. Tools Manuf. 45 (2005) 1635–1639. https://doi.org/10.1016/j.ijmachtools.2004.11.026.

[11] S.J. Barnes, A.R. Bhatti, A. Steuwer, R. Johnson, J. Altenkirch, P.J. Withers, Friction Stir Welding in HSLA-65 Steel: Part I. Influence of Weld Speed and Tool Material on Microstructural Development, Metall. Mater. Trans. A. 43 (2012) 2342–2355. https://doi.org/10.1007/s11661-012-1110-z.

[12] V.N. Malyshev, Tribological aspects in friction stir welding and processing, in: Adv. Frict. Weld. Process., Elsevier, 2014: pp. 329–386. https://doi.org/10.1533/9780857094551.329.

[13] S. Hanke, G.V.B. Lemos, L. Bergmann, D. Martinazzi, J.F. dos Santos, T.R.

Strohaecker, Degradation mechanisms of pcBN tool material during Friction Stir Welding of Ni-base alloy 625, Wear. 376–377 (2017) 403–408. https://doi.org/10.1016/j.wear.2017.01.070.

[14] Y. Zhang, Y.S. Sato, H. Kokawa, S.H.C. Park, S. Hirano, Stir zone microstructure of commercial purity titanium friction stir welded using pcBN tool, Mater. Sci. Eng. A. 488 (2008) 25–30. https://doi.org/10.1016/j.msea.2007.10.062.

[15] D.J. Shindo, A.R. Rivera, L.E. Murr, Shape optimization for tool wear in the friction-stir welding of cast AI359-20 % SiC MMC, J. Mater. Sci. 37 (2002) 4999–5005. https://doi.org/10.1023/A:1021023329430.

[16] M. Almoussawi, A.J. Smith, M. Faraji, Wear of Polycrystalline Boron Nitride Tool During the Friction Stir Welding of Steel, Metallogr. Microstruct. Anal. 7 (2018) 252–267. https://doi.org/10.1007/s13632-018-0439-0.

[17] M. Collier, R. Steel, T.W. Nelson, C. Sorensen, S. Packer, Grade Development of Polycrystalline Cubic Boron Nitride for Friction Stir Processing of Ferrous Alloys, Mater. Sci. Forum. 426–432 (2003) 3011–3016. https://doi.org/10.4028/www.scientific.net/MSF.426-432.3011.

[18] R. Rai, A. De, H.K.D.H. Bhadeshia, T. Debroy, Review: friction stir welding tools, Sci. Technol. Weld. Join. 16 (2011) 325–342. https://doi.org/10.1179/1362171811Y.0000000023.

[19] J.A. Avila, R.A.R. Giorjao, J. Rodriguez, E.B. Fonseca, A.J. Ramirez, Modeling of thermal cycles and microstructural analysis of pipeline steels processed by friction stir processing, Int. J. Adv. Manuf. Technol. 98 (2018) 2611–2618. https://doi.org/10.1007/s00170-018-2408-9.

[20] J.A. Avila, E. Lucon, J.W. Sowards, P.R. Mei, A.J. Ramirez, Assessment of Ductile-to-Brittle Transition Behavior of Localized Microstructural Regions in a Friction-Stir Welded X80 Pipeline Steel with Miniaturized Charpy V-Notch Testing, Metall. Mater. Trans. A. 47 (2016) 2855–2865. https://doi.org/10.1007/s11661-016-3473-z.

[21] H.B. Schmidt, J.H. Hattel, Thermal modelling of friction stir welding, Scr. Mater. 58 (2008) 332–337. https://doi.org/10.1016/j.scriptamat.2007.10.008.

[22] R.A.R. Giorjão, V.F. Pereira, M. Terada, E.B. da Fonseca, R.R. Marinho, D.M. Garcia, A.P. Tschiptschin, Microstructure and mechanical properties of friction stir welded 8 mm pipe SAF 2507 super duplex stainless steel, J. Mater. Res. Technol. (2018) 2–8. https://doi.org/10.1016/j.jmrt.2018.01.002.

[23] P. Shahi, M. Barmouz, P. Asadi, Force and torque in friction stir welding, in: Adv. Frict. Weld. Process., Elsevier, 2014: pp. 459–498.

https://doi.org/10.1533/9780857094551.459.

[24] R. Giorjao, E. Fonseca, J. Avila, E. Monlevade, A. Tschiptschin, Investigation of material flow and thermomechanical behavior during friction stir welding of an AZ31B alloy for threaded and unthreaded pin geometries using computational solid mechanics simulation, Proc. Inst. Mech. Eng. Part C J. Mech. Eng. Sci. (2020) 095440622096254. https://doi.org/10.1177/0954406220962540.

[25] A.F. Hasan, C.J. Bennett, P.H. Shipway, A numerical comparison of the flow behaviour in Friction Stir Welding (FSW) using unworn and worn tool geometries, Mater. Des. 87 (2015) 1037–1046. https://doi.org/10.1016/j.matdes.2015.08.016.

[26] H. Schmidt, J. Hattel, J. Wert, An analytical model for the heat generation in friction stir welding, Model. Simul. Mater. Sci. Eng. 12 (2004) 143–157. https://doi.org/10.1088/0965-0393/12/1/013.

[27] L. Fratini, G. Buffa, D. Palmeri, J. Hua, R. Shivpuri, Material flow in FSW of AA7075–T6 butt joints: numerical simulations and experimental verifications, Sci. Technol. Weld. Join. 11 (2006) 412–421. https://doi.org/10.1179/174329306X113271.

[28] R. Nandan, G.G. Roy, T.J. Lienert, T. Debroy, Three-dimensional heat and material flow during friction stir welding of mild steel, Acta Mater. 55 (2007) 883–895. https://doi.org/10.1016/j.actamat.2006.09.009.

[29] R. Nandan, G.G. Roy, T.J. Lienert, T. Debroy, Numerical modelling of 3D plastic flow and heat transfer during friction stir welding of stainless steel, Sci. Technol. Weld. Join. 11 (2006) 526–537. https://doi.org/10.1179/174329306X107692.

[30] P. Asadi, M. Akbari, H. Karimi-Nemch, Simulation of friction stir welding and processing, in: Adv. Frict. Weld. Process., Elsevier, 2014: pp. 499–542. https://doi.org/10.1533/9780857094551.499.

[31] K. Zhu, C. Oberbillig, C. Musik, D. Loison, T. Iung, Effect of B and B+Nb on the bainitic transformation in low carbon steels, Mater. Sci. Eng. A. 528 (2011) 4222–4231. https://doi.org/10.1016/j.msea.2011.02.022.

[32] G.F. Melloy, P.R. Summon, P.P. Podgursky, Optimizing the boron effect, Metall. Trans. 4 (1973) 2279–2289. https://doi.org/10.1007/BF02669367.